Biosensors and Bioelectronics 126 (2019) 36–43

Contents lists available at ScienceDirect

Biosensors and Bioelectronics

journal homepage: www.elsevier.com/locate/bios

Vertical flow-based paper immunosensor for rapid electrochemical and colorimetric detection of influenza virus using a different pore size sample pad

Jyoti Bhardwaj[a], Abhinav Sharma[b], Jaesung Jang[a,c,*]

[a] Department of Biomedical Engineering, Ulsan National Institute of Science and Technology (UNIST), Ulsan 44919, Republic of Korea
[b] School of Materials Science and Engineering, UNIST, Ulsan 44919, Republic of Korea
[c] School of Mechanical, Aerospace and Nuclear Engineering, UNIST, Ulsan 44919, Republic of Korea

ARTICLE INFO

Keywords:
Vertical flow assay
Electrochemical sensor
Colorimetric sensor
Sandwich immunoreaction
H1N1 influenza virus
Paper sensors

ABSTRACT

We present a novel vertical flow-based paper immunosensor for the rapid and sensitive electrochemical and colorimetric detection of influenza H1N1 viruses using a different pore size (DP) sample pad. The DP sample pad consisted of two different pore size papers: larger pores (diameter: 11 μm) facing the inlet, and smaller pores (diameter: 0.45 μm) facing the conjugate pad. This sample pad offered moderate and uniform flows, and hence concentrated horseradish peroxidase tagged antibodies (HRP-Abs)-H1N1 complexes from 40 μL of sample volumes on a conjugate pad for 2 min after sample injection, thereby providing fast detection (6 min for both detection methods) with 100 μL of flushing afterwards, high sensitivity, and the simplicity of the sensor. The filtration characteristics of the DP sample pad were evaluated using fluorescent beads, indicating that only small-sized bio-particles such as viruses can pass through the sample pad. Sandwich immunoreactions of HRP-Ab-H1N1-Ab were performed on the gold paper electrode of the immunoStrip, which was determined by electrochemical impedance spectroscopy (EIS) measurements. Simultaneously, the color signal of free HRP-Ab captured on the colorimetric zone was obtained using a scanner, and the intensity was analyzed using ImageJ. This immunosensor detected H1N1 virus concentration as low as 3.3 plaque forming units (PFU)/mL (phosphate buffer saline; PBS) and 4.7 PFU/mL (saliva) by EIS, and 1.34 PFU/mL (PBS) and 2.27 PFU/mL (saliva) by the colorimetric method. Furthermore, integrating these two detection methods can reduce false results with double assurance, and this device can provide a simple and economical on-site detection platform.

1. Introduction

The influenza virus is one of the biggest threats to human health. Because of their host-range diversity, influenza A viruses can lead to the development of pandemics (Taubenberger and Morens, 2010). Among the influenza A viruses, the H1N1 subtype was first isolated from swine in 1930 (van der Meer et al., 2010), and epidemics and pandemics of H1N1 viruses have caused significant socio-economic losses worldwide, thus necessitating rapid and reliable sensors of the viruses for on-site detection and rapid treatment (Nikitin et al., 2014).

Recently, paper-based immunosensors have gained much attention for the development of point-of-care testing kits (Jauset-Rubio et al., 2016; Sajid et al., 2015) using the lateral flow assay (LFA) technology. The LFA-based paper sensors generally consist of a sample pad, a conjugate pad, nitrocellulose (NC) membrane, and an absorption pad. In these sensors, test analytes pass horizontally from one end (the sample pad) to the other end (the test section and the absorption pad) by capillary force, and antigens bind with labeled antibodies on the conjugation pad for a sensitive detection.

Many different principles such as colorimetric, fluorometric, chemiluminescent, and electrochemical methods have been successfully implemented in the paper-based immunosensors. Among these methods, electrochemical detection is an attractive option owing to its ability to perform quantitative analysis with less background noises (Liu et al., 2014). Several LFA-based electrochemical sensors have shown a one-step POC biosensor, providing relatively short assay times (approximately 10–20 min), low-cost analysis, simple handling, and ease of mass production (Du et al., 2012; Sinawang et al., 2016; Zhu et al., 2014). However, the LFA technology possesses several limitations, such as a relatively low sensitivity, limited sample volume, and

* Corresponding author at: School of Mechanical, Aerospace and Nuclear Engineering, Ulsan National Institute of Science and Technology (UNIST), Ulsan 44919, Republic of Korea.
E-mail address: jjang@unist.ac.kr (J. Jang).

https://doi.org/10.1016/j.bios.2018.10.008
Received 17 July 2018; Received in revised form 3 October 2018; Accepted 3 October 2018
Available online 19 October 2018
0956-5663/

difficulties in making multiple measurements (Posthuma-Trumpie et al., 2009; Sajid et al., 2015; Oh et al., 2013). Furthermore, the LFA-based sensors are more susceptible to inaccurate detections if applied to real samples (Lim et al., 2017; Zhu et al., 2014).

In recent years, three-dimensional microfluidic paper devices have been developed to improve the LFA-based sensors (de Oliveira et al., 2017; Han et al., 2016; He et al., 2015), and Oh et al. (2013) presented a vertical flow assay (VFA)-based colorimetric immunosensor using the sandwich ELISA for the sensitive detection of C-reactive protein. This immunosensor contained flow control components in addition to a sample pad, a conjugate pad, and NC membrane, and demonstrated more rapid results (within a few minutes), a wide detection range, good sensitivity, and required relatively small sample volumes (Clarke et al., 2017; Oh et al., 2013).

Herein, we present a VFA-based paper immunosensor using a different pore size (DP) sample pad for the electrochemical and colorimetric detection of the influenza virus H1N1 in both the standard buffer solution and saliva samples. Colorimetric paper-based sensors generally can offer positive or negative results on a visual basis without any complicated instrumentation, and electrochemical impedance spectroscopy (EIS) enables the detection of low concentrations of analytes in which the colorimetric method may fail, along with quantitative and portable results (Adkins et al., 2017). Therefore, the simultaneous use of both the detection methods on the same platform can overcome the disadvantages associated with using an individual technique.

Controlling the flow speed and quantity of a sample solution through the paper sensors significantly influences binding efficiency between the labeled antibodies and antigens, and hence the sensitivity and accuracy of the sensors. Oh et al. (2013) used hydrophobic flow control films and asymmetric membranes, in addition to the primary components, to control the flows and to enhance the sensitivity. Here, a DP sample pad whose pore sizes on the upper and lower sides were 11 μm and 0.45 μm, respectively, was used. Although cellulose and glass fiber sample pads have been extensively used in paper-based sensors, the effects of a DP sample pad on the sensor performances have received little attention to date. This sample pad increased the binding efficiency of antigen-horseradish peroxidase-tagged antibodies (HRP-Abs) on a conjugate pad and concentrated the antigen–antibody complexes by providing the optimal residual time, thereby providing fast detection and high sensitivity. Furthermore, this sample pad can act as a filter to pass small-sized biological particles such as viruses, while retaining larger particles, which would be useful for the detection of complex fluids or air samples (Hong et al., 2016).

The present VFA sensor consists of a DP sample pad, a conjugate pad, an NC membrane strip, and an absorption pad, all of which are vertically stacked one upon the other onto a polyester backing film. The hydrophilic colorimetric zone and the three-electrode area were defined on an NC membrane strip by wax printing. We explore the effects of pore sizes of a DP sample pad on the detection time and accuracy, along with the selectivity, stability, and reproducibility of the sensors.

2. Materials and methods

2.1. Materials and reagents

An NC membrane (10600002), Whatman filter papers (pore diameter: 11 μm; WHA1001125), polytetrafluorethylene membrane filters (pore diameter: 0.45 μm; HP045047D), and an A4-sized adhesive polyester backing sheets were obtained from General Electric Healthcare (South Korea). Glass-fiber conjugate pads (G041) were acquired from Millipore (Billerica, MA). Conductive carbon paste (DC-21, sheet resistance: 20–25 Ω/square, thickness: 20 μm), and Ag/AgCl ink (011464) were obtained from Dozen Tech (South Korea) and BAS Inc. (Tokyo, Japan), respectively. Sucrose (S1030), 1 × phosphate buffered saline (PBS; pH: 7.4), and tween-20 (P2006) were procured from Biosesang Inc. (South Korea). N-(3-dimethylaminopropyl)-N′-ethylcarbodiimide hydrochloride (EDC; 03449), N-hydroxysuccinimide (NHS; 130672), bovine serum albumin (BSA; A2153), Triton X-100 (93443), 11-mercaptoundecanoic acid (MUA; 674427), Tetramethylbenzidine substrate (TMB; T0440), hydroquinone (HQ; H9003-HQ), and methylene blue (MB; M9140) dye were purchased from Sigma-Aldrich (USA). Anti-goat IgG (Ab-C) (ab97096) was obtained from Abcam (USA). Anti-influenza A HA antibody (Ab-E) (AB1074) and HRP-tagged anti-influenza A HA antibody (HRP-Ab) (60–130) were purchased from Merck Millipore and Fitzgerald (USA), respectively. Red fluorescent polymer microspheres [diameters: 1 μm (R0100) and 0.30 μm (R300)] were purchased from Thermo Scientific (USA). Influenza A virus H1N1 (KBPV-VR-76), Influenza B virus (KBPV-VR-34), and Adenovirus A virus (KBPV-VR-4) were procured from the bank of pathogenic viruses (South Korea). MS2 bacteriophage (ATCC® 15597-B1™) was procured from Koram Biogen Corp. (South Korea). Deionized water (dH_2O) was used in all experiments.

2.2. Preparation and assembly of the VFA sensor

The VFA sensor (L × W; 32 mm × 22 mm) was fabricated by stacking a DP sample pad, a conjugate pad, and an NC membrane strip with double-sided adhesive tapes between each. Holes were created in specific locations of the adhesive tapes (1, 2, and 3) for the flow of the antigen-containing solution during assay (Fig. 1(A) and (B)).

A DP sample pad (L × W; 26 mm × 12 mm) was prepared by attaching a Whatman filter paper to a polytetrafluorethylene membrane filter using double-sided adhesive tape, with the Whatman filter paper facing the sample inlet. An NC membrane strip was patterned by wax printing to define the hydrophilic colorimetric zone and the three-electrode area (L × W; 22 mm × 12 mm). The patterned NC membrane strip was heated at 90 °C on a hot plate for 2 min to melt the patterned wax. Gold (thickness: 100 nm) was deposited by e-beam evaporation for the working electrode (GPE: gold paper electrode). Carbon paste and Ag/AgCl were deposited by stencil printing for the counter and reference electrodes, respectively, and these electrodes were separated from the working electrode by a semi-hydrophobic barrier. The colorimetric zone consisted of a circular paper surface (diameter: 6 mm) without gold on it, and it was created by wax patterning to define the circular hydrophilic zone. The DP sample pad and the patterned NC membrane strip were pretreated with PBS containing 1% BSA, 0.01% Tween-20%, and 0.25% Triton X-100 for 10 min, dried in an oven for 30 min at 45 °C, and stored at room temperature. The immobilization of Ab-E and BSA on the GPE and Ab-C on the colorimetric zone was made, as described in the Supplementary information (Fig. S1). The NC membrane strip was subsequently attached to a Whatman filter paper (an absorption pad) and polyester backing film, and stored at 4 °C until further use.

The glass-fiber conjugate pad (L × W; 26 mm × 12 mm) was treated with PBS containing 2% sucrose, 1% BSA, 0.01% Tween-20%, and 0.25% Triton X-100 for 10 min (Lee et al., 2013). The pad was subsequently dried in an oven for 30 min at 45 °C, and stored at room temperature. The desired volume (30 μL) of HRP-Ab 1000-fold diluted in PBS with 1% BSA and 2% sucrose solution was subsequently dispensed by a pipette onto the conjugate pad, which was dried at room temperature subsequently and stored at 4 °C. The sucrose solution contributes to the optimal release of antibodies from the conjugation pad (Föllscher, 2013).

2.3. Optimization of sample flow time and filtration of the DP sample pad

The sample flow speed and quantity through the paper substrate are critical for the sensitivity and accuracy of the sensors. In this study, the DP sample pad acted as a flow control component, and the sample flow time was compared using 0.1% MB dye for three different types of sample pads: a DP sample pad with large pores (11 μm) on the upper side and small pores (0.45 μm) on the lower side (DP1 pad), a DP pad

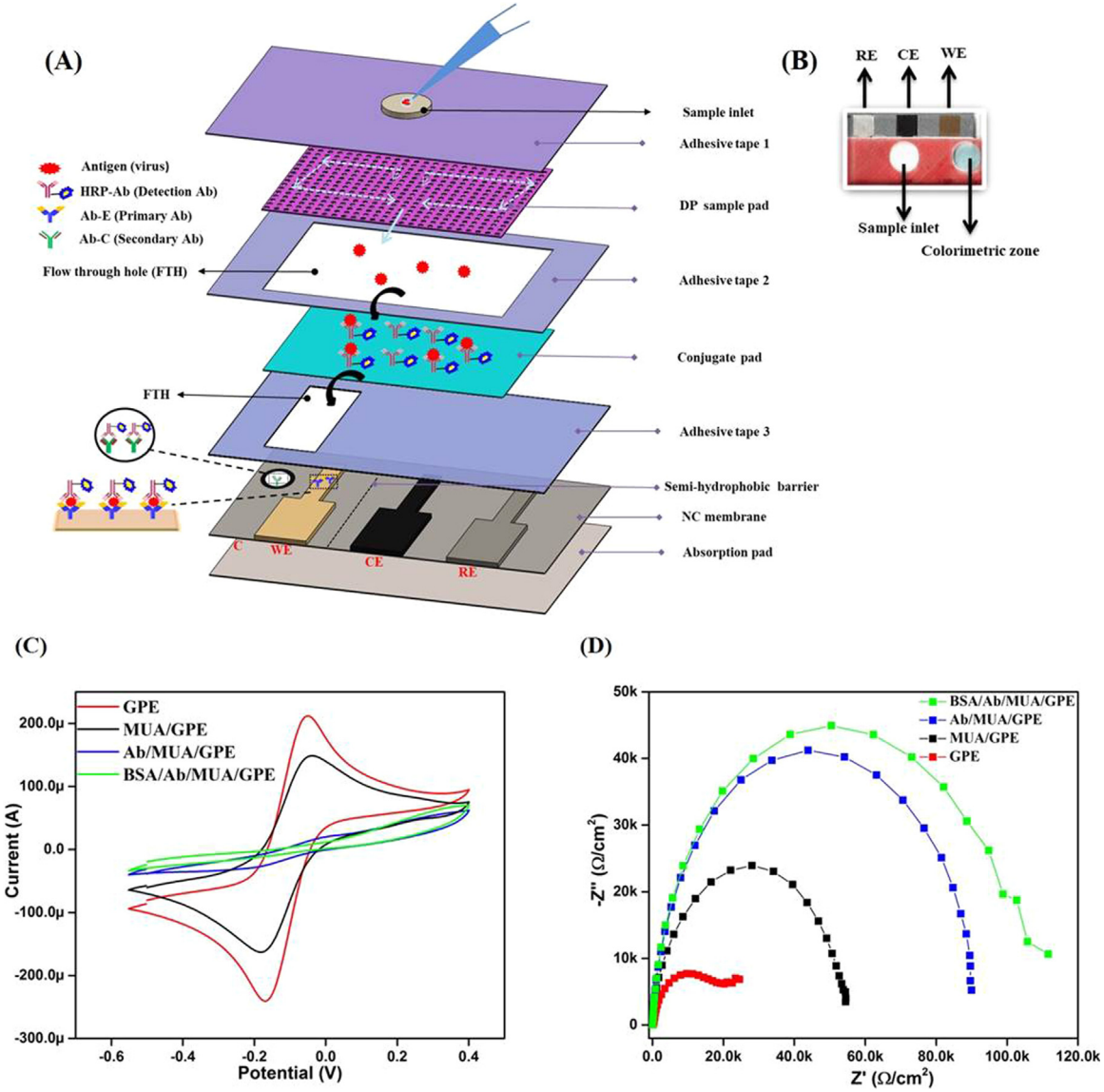

Fig. 1. (A) Schematic of the integrated vertical flow assay device for dual detection. The sample pad consists of two different pore size papers: the upper one is the larger pore sized (11 μm) and the lower one is smaller pore sized (0.45 μm). (B) Photograph of a representative VFA device. (C) Cyclic voltammograms of GPE, MUA/GPE, Ab/MUA/GPE, and BSA/Ab/MUA/GPE. (D) Electrochemical impedance spectra of GPE, MUA/GPE, Ab/MUA/GPE, and BSA/Ab/MUA/GPE in the presence of 1× PBS containing 5 mM $(Fe(CN)_6)^{-3/-4}$ and 0.5 M KCl as a redox mediator.

with small pores (0.45 μm) on the upper side and large pores (11 μm) on the lower side (DP2 pad), and a large pore size (11 μm) sample pad (LP pad). We measured the time of sample flows through these sample pads to the conjugate pad and the NC membrane by the visual observation of the blue color (MB dye).

The filtration behavior of the DP1 sample pad was also investigated using red polystyrene beads of different diameters (1 μm (10^6 mL^{-1}) and 0.3 μm (10^6 mL^{-1})). We mixed both and dropped 40 μL of the mixture on the DP sample pad, and acquired fluorescence images. Subsequently, 100 μL of PBS was added to the DP sample pad after 2 min and fluorescence images were captured by detaching the layers of the VFA device individually. The fluorescence images were obtained using an epifluorescence microscope (CELENA Digital Imaging system, Logos Biosystems, USA) with an exposure time of 100 ms and a 20× objective lens. The quantitative analysis for the fluorescence images of the beads on paper was conducted using ImageJ.

2.4. Coupled impedimetric and colorimetric measurements

A 40 μL aliquot of the PBS sample or spiked saliva sample containing various concentrations of influenza H1N1 viruses was applied to the sample inlet, and it started to flow vertically to initiate and complete the binding with HRP-Abs on a conjugate pad for 2 min. Subsequently, 100 μL of PBS was applied through the sample inlet to continue the flow of antigen-HRP-Ab complexes from the conjugate pad to the NC membrane, and incubated for an additional 4 min. To prevent the interference of the colorimetric substrate during the electrochemical analysis, the colorimetric zone was separated from the three-electrode zone. For electrochemical detection, 100 μL of 0.1 M PBS containing 2 mM HQ and 1.5 mM H_2O_2 (a substrate solution for electrochemical detection) was added into the inlet. Subsequently, a strong redox signal on the GPE from the electro-reduction of the H_2O_2 reaction catalyzed by HRP was obtained depending on the concentration of the virus samples, and impedimetric measurements were performed using an electrochemical analyzer (Autolab PGSTAT204, Metrohm, the Netherlands) and NOVA 1.10. The charge transfer resistance (R_{CT}) was

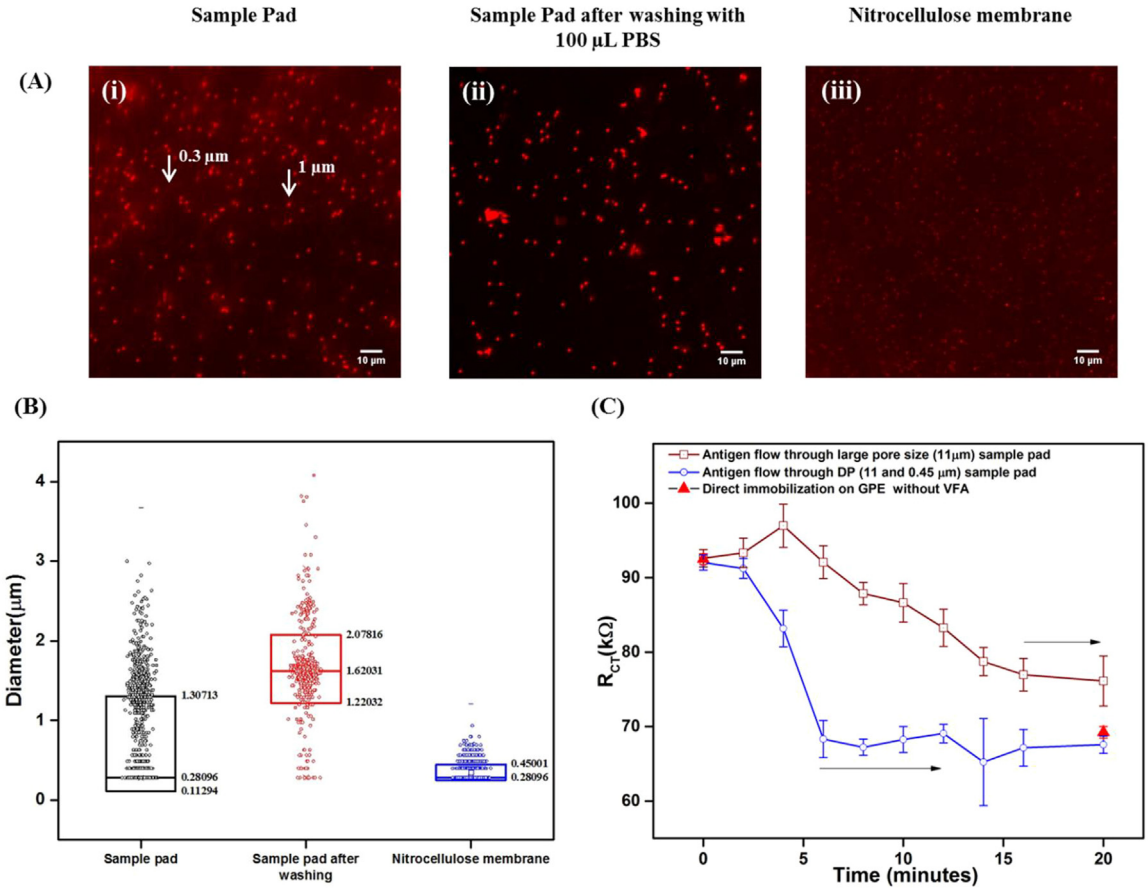

Fig. 2. (A) Fluorescence images of polystyrene beads on a sample pad (or polytetrafluorethylene membrane filters) (i) before washing, (ii) after washing with 100 µL of PBS, and (iii) on a nitrocellulose membrane after washing with 100 µL of PBS. (B) Box graph to analyze the particle size based on the fluorescence images using ImageJ. (C) Pore size effects of two different sample pads, a single large pore size (11 µm) sample pad, and a different pore size (DP) sample pad with large pores (11 µm) on the upper side and small pores (0.45 µm) on the lower side, by measuring the charge transfer resistances (R_{CT}) with time. The error bars represent the standard deviations of three independent measurements.

determined using the Nova software, where the diameter of a semicircle indicates the R_{CT} according to the electrochemical circle fit.

Simultaneously, 10 µL of TMB substrate was applied on the colorimetric zone and the photograph of the colorimetric zone was obtained using a digital scanner (Samsung SCX-3205). After obtaining the photos, color intensity was measured from 16 bit Grayscale images using ImageJ intensity function. To measure the signal from the colorimetric zone, a circle 5 mm in diameter was used as a uniform region of interest.

3. Results and discussion

3.1. Electrochemical behavior of modified immunoelectrodes

Fig. 1(C) shows the cyclic voltammograms with the modification of GPE: MUA/GPE, Ab/MUA/GPE, and BSA/Ab/MUA/GPE. The peak current decreased to 147 µA after the immobilization of MUA solution, which indicates the formation of a stable and well-ordered self-assembled monolayer (SAM) onto the gold electrode. Contact angle measurements and surface characterization of the MUA-treated GPE also supports the formation of stable and densely packed arrays of thiols on the GPE (Fig. S2). The peak current for Ab/MUA/GPE was found to decrease (17.9 µA) because of the insulating behavior of the antibodies. After the BSA immobilization, the current further decreased to 9.08 µA due to the insulating behavior of BSA. The differential pulse voltammetry (DPV) measurements were in good agreement with the cyclic voltammetry (CV) data (Fig. S3(A)); the scan rate effects for the MUA/GPE are provided in the Supplementary information (Fig. S3(B)).

The interfacial changes induced by the biological recognition events were studied by EIS (Fig. 1(D)). The R_{CT} for the GPE increased from 18.2 kΩ to 57.8 kΩ after the MUA deposition, and to 89.3 kΩ after the antibody immobilization, showing the good binding of antibody on the gold electrode. A further increase in the R_{CT} value of 94.48 kΩ for the BSA/Ab/MUA/GPE indicates that BSA covered the non-specific sites of the Ab/MUA/GPE and impeded the electron transfer.

3.2. Visual optimization of sample flow time using different pore size sample pads

The optimal sample volume and flow speed are critical factors for the effective binding of antigen with HRP-Abs on the conjugate pad, and hence the sensitivity, accuracy, and detection time. We investigated the effects of different pore sizes of the sample pads on the flow speed of samples using 40 µL of 0.1% MB dye as an indicator. The optimal sample volume of 40 µL was used for initiating the antigen binding with HRP-Abs on the conjugate pad (Section 3.3).

The LP sample pads showed fast and non-uniform flows on the conjugate pad and the NC membrane, which can cause false results and slow detections (Section 3.3). A DP2 sample pad was inefficient for a rapid detection because the dye remained in the sample pad even after 2 min, thus requiring more than 2 min to flow from the sample pad to the conjugate pad. By contrast, the DP1 sample pad showed moderate and uniform flow on the conjugate pad within 1 min 20 s (Movie), which may be due that the smaller pores on the bottom can pull down

the solution fast from the larger pores (Cummins et al., 2017) in comparison to the DP2 sample pad (Movie). Unlike the LP sample pad, the dye covered the conjugate pad area completely and uniformly within 1 min 20 s without contacting the NC membrane (Movie). Moreover, this moderate flow and uniform coverage on the conjugate pad without contacting the NC membrane may help the preconcentration of dye (or antigen–antibody complexes) on the conjugate pad for another period of time (~40 s). Therefore, a total of 2 min was spent to pass the limited amount of sample volume (40 μL) and to generate the proper antigen-HRP-Ab reaction in the case of antigens. After 2 min, 100 μL of PBS was added into the sample inlet to wash off the remaining MB dye on the sample pad and move the dye to the NC membrane. Subsequently, the dye flowed through the hole in adhesive tape 3, resulting in a uniform blue line on the NC membrane (Movie). This uniform blue line on the NC membrane implies that sufficient amount of antigen-HRP-Ab complexes will combine with Ab-E on the GPE, while unbound HRP-Abs will bind with Ab-C on the colorimetric zone.

Furthermore, the DP1 sample pad can act as a filter that facilitates smaller particles to pass through and larger particles to be collected on the sample pad (Fig. 2(A)). A mixture of two different size (diameters: 1 μm and 0.3 μm) fluorescent beads were applied onto the DP sample pad (Fig. 2(A) (i)). After washing with PBS (Fig. 2(A) (ii)), the 1 μm diameter beads or aggregated beads remained on the sample pad, and smaller beads passed through the sample pad to the lower NC membrane (Fig. 2(A) (iii)). The quantitative analysis of the fluorescence images was performed with the particle size analyzer option of ImageJ. The analysis showed that the average diameters of the red polystyrene beads remaining on the sample pad were 1.3 μm and 0.28 μm before washing, 1.2, 1.6, and 2.0 μm after washing, and 0.28 μm and 0.45 μm on the NC membrane (Fig. 2(B)). This sample pad would be useful for detecting viruses from a mixture of different sized particles such as complex fluids or air samples.

3.3. Sample volume and pore size effects using EIS

The sensor performances depend significantly on the amount of sample volume. A series of 10, 20, 30, 40, 50, and 60 μL of sample solutions (Virus concentration: 2500 PFU mL^{-1}) were applied to the DP1 sample pads respectively. For EIS measurements, the concentration of redox substrates (HQ and H_2O_2) were also optimized using CV (Fig. S4), and 40 μL sample volume showed a maximum decrease in the R_{CT} values (Fig. S5).

To determine the pore size effects of the sample pads, 40 μL of H1N1 virus suspensions (100 PFU mL^{-1}) were applied directly on the GPE (without the sample pads) and both LP and DP1 sample pads, and the R_{CT} values were measured using EIS (Fig. 2(C)). In the LP sample pad, we observed an increase in R_{CT} up to the initial 5 min, and subsequently a continuous and monotonous decrease in R_{CT} values up to 15 min, and the R_{CT} values remained constant after 15 min. The initial increase in the R_{CT} values might be due to the binding of free H1N1 viruses (Fig. S6) on the GPE without the formation of sandwich complexes with HRP-Ab, which degraded the sensitivity and accuracy of the sensors. In fact, the resistance values at 20 min were larger than those observed in the direct immobilization on the GPE, underestimating the virus concentration of the sample: approximately 50% underestimation in this virus concentration. The continuous and slow decrease in the R_{CT} values from 5 to 15 min implies that the application of 100 μL PBS caused the smaller number of created HRP-Ab-virus complexes to move slowly to the GPE through the paper substrates previously wetted by the initial sample injection. The DP2 sample pad could provide good sensitivity; however, as shown from the visual optimization study of the sample flow time (Movie), 40 μL of dye could not reach the conjugate pad even after 2 min. This may result in a longer response time.

In contrast, in case of the DP1 sample pads, the R_{CT} values remained unchanged for the initial 2 min, because the 40 μL samples required 1 min 20 s to travel from the sample pad to the conjugate pad, and another 40 s for antigen binding with HRP-Abs on the conjugate pad. After applying 100 μL of PBS subsequently, the R_{CT} values started to decrease rapidly owing to the formation of sandwich complexes on the GPE, and became constant after 5 min, implying that no more H1N1-HRP-Ab complexes combined with Ab-E in the working electrode. The application of 100 μL PBS to initiate the flow of antigen-HRP-Ab complexes from the conjugate pad to the NC membrane and test section is an essential step in this VFA sensor, which was more effective in the VFA-based sensors owing to gravity, unlike the LFA. The small pore size (0.45 μm) provided a moderate and uniform flow for a 5 min detection, and passed single influenza viruses and their aggregates as well, where the diameter of single influenza viruses is approximately 100 nm. This pore size can also be used for the detection of many different-sized viruses. Furthermore, the R_{CT} values at 5 min were close to those observed in the direct immobilization on the GPE, demonstrating the accuracy of the measurements (Relative differences: 1.1%).

3.4. Impedimetric analysis

Impedimetric measurements were performed using 2 mM HQ and 1.5 mM H_2O_2 in the frequency ranging from 0.1 Hz to 100 kHz for 6 min after applying the H1N1 virus samples (in either PBS or saliva) to the sample inlet. The preparation of standard samples in PBS and spiked saliva samples are provided in Supplementary information. The optimization of response time was also performed (Fig. S7(A)). Fig. 3(A) and (B) show the R_{CT} graphs for the detection of H1N1 viruses in PBS and saliva, respectively, with representative impedance response graphs in the insets. The measured R_{CT} values are tabulated in Table S1. An H1N1 concentration-dependent decrease in the R_{CT} value is shown with $R^2 = 0.98$ in PBS and $R^2 = 0.97$ in the saliva samples. Increasing the H1N1 virus concentration led to a decrease in the semi-circle diameter in the Nyquist plots. This is due to the increase in the H1N1-HRP-Ab concentration (Kim et al., 2016), because HRP provides redox activity using HQ as a mediator and H_2O_2 as the substrate. This is consistent with the DPV measurements, where the peak current increased with the increasing concentration of H1N1 virus owing to the enzymatic reactions with the HRP substrate (Fig. S7(B)).

From the calibration graphs, the limit of detection (LOD) by the electrochemical detection were calculated as 3.3 PFU mL^{-1} in PBS and 4.7 PFU mL^{-1} in the saliva samples based on three times the standard deviation of blank samples. Although nasal samples are most commonly used for the detection of respiratory viruses in clinics, saliva samples are easier and safer to obtain, and might be acceptable for screening in case it is not easy to take nasal samples, for example at home (Robinson et al., 2008). Considering that the infectious dose of H1N1 viruses in saliva and nasal secretions is typically 10^3–10^5 $TCID_{50}$ mL^{-1} (Yezli and Otter, 2011), the present sensor is highly sensitive. In comparison to the previously reported electrochemical and colorimetric sensors for the detection of influenza viruses (Table S2), the present VFA sensor using the DP sample pad demonstrated increased sensitivity, along with simplicity in structure and rapid detection time (6 min). Moreover, dual measurements of the present device can offer more reliability for public use.

3.5. Colorimetric analysis

A series of H1N1 influenza virus in PBS and 80% saliva samples spiked with concentrations of 0–10,000 PFU mL^{-1} were applied to the sample inlets. After 6 min, the color intensity on the colorimetric zone was recorded (Fig. 4(A)). The color series showed typical responses with increasing H1N1 virus concentrations from 0 to 10,000 PFU mL^{-1}. The color intensity decreased as the virus concentration increased because a less amount of HRP-Ab free of H1N1 was captured on the colorimetric zone. Fig. 4(B) shows a linear relationship between the color intensity and the logarithmic concentration, where $R^2 = 0.97$, and the LOD was found to be 1.34 PFU mL^{-1}. Fig. 4(C) shows the linear

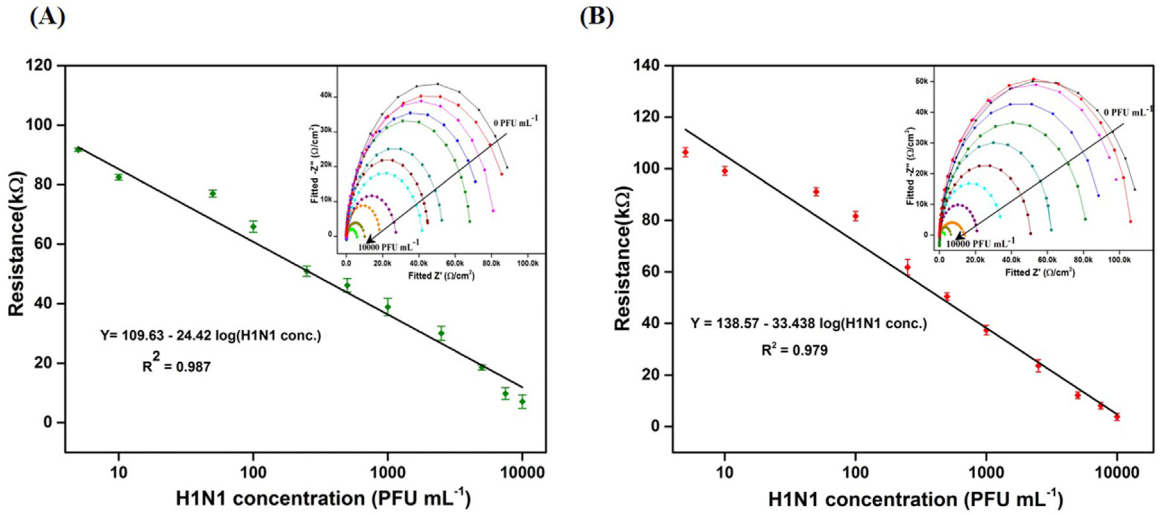

Fig. 3. Calibration graphs showing the charge transfer resistance values as functions of the concentrations of H1N1 virus in (A) PBS and (B) spiked saliva samples. The insets show the Nyquist plots recorded in a redox probe solution in the presence of 0.1 M PBS containing 1.5 mM H_2O_2 with 2 mM HQ for the detection of H1N1 virus concentrations ranging from 0 to 10,000 PFU mL^{-1}. The error bars represent the standard deviations of three independent measurements.

calibration curve rendered from the saliva samples spiked with varying H1N1 concentrations, where R^2 = 0.98 and the LOD was 2.27 PFU mL^{-1}. Considering that most commercialized ELISA kits can detect H1N1 concentrations in the range of $10^{4.6}$–$10^{7.6}$ EID_{50} mL^{-1} with a detection limit of $10^{4.6}$ EID_{50} mL^{-1} (i.e., rapid AIV Ag Test Kit (RG1501MH), Bionote), and the detection limit of a dipstick LFA-based colorimetric immunosensor is 0.7×10^7 PFU mL^{-1} (Anderson et al., 2017), the present results show that this strip can potentially be used as a simple, rapid (~6 min), and low-cost platform for the detection of H1N1 viruses.

3.6. Reproducibility, selectivity, and stability

To evaluate the reproducibility of the immunosensors, a series of five different devices were prepared for the detection of 2500 PFU mL^{-1} of H1N1 virus (Fig. 5(A)). The relative standard deviation (RSD) of the measurements for the five devices was 4.24%, indicating that the precision and reproducibility of the immunosensors was acceptable. The selectivity of the proposed immunosensors was also determined using adenovirus, influenza B viruses, and MS2 phages (Fig. 5(B)). The resistances of the BSA/Ab/MUA/GPE decreased to

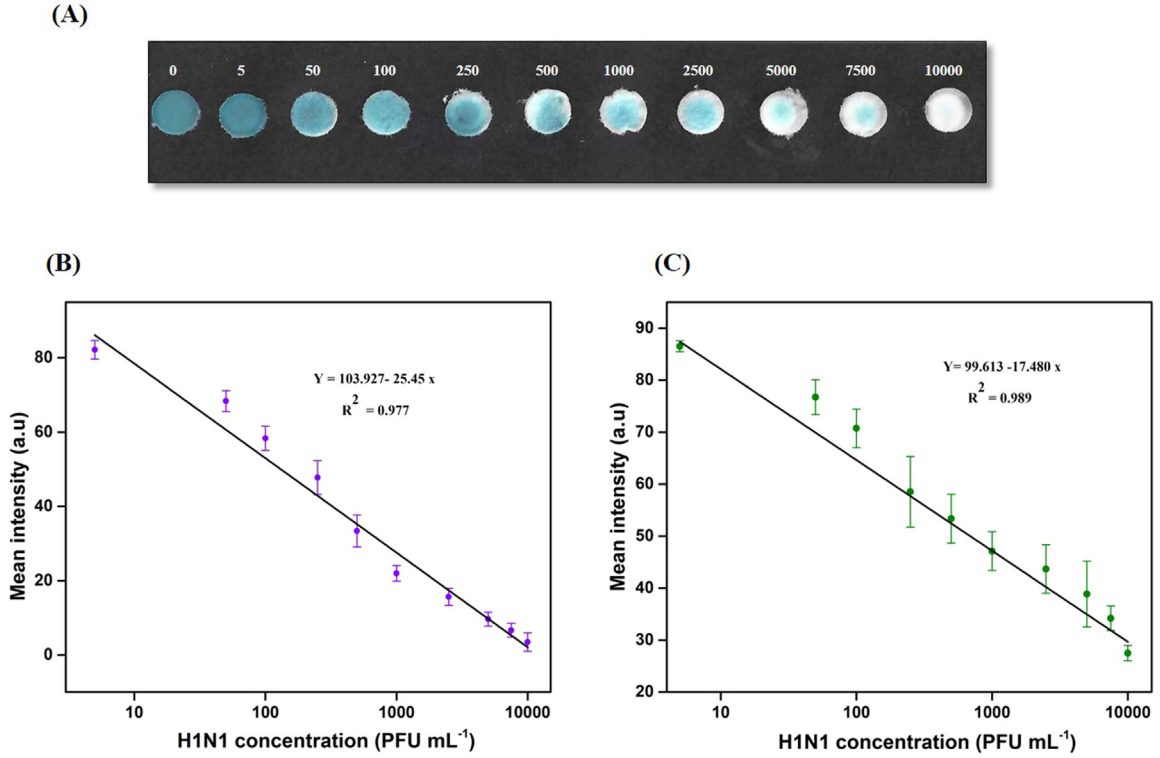

Fig. 4. (A) Color bars represent the color intensity of H1N1 standard solutions with varying concentrations (PFU mL^{-1}) in the presence of TMB substrate. Calibration graphs were based on the mean intensity of the control zone plotted against the various concentrations of H1N1 in (B) PBS and (C) spiked saliva samples, ranging from 0 to 10,000 PFU mL^{-1}. The error bars represent the standard deviations of three independent measurements. (For interpretation of the references to color in this figure legend, the reader is referred to the web version of this article).

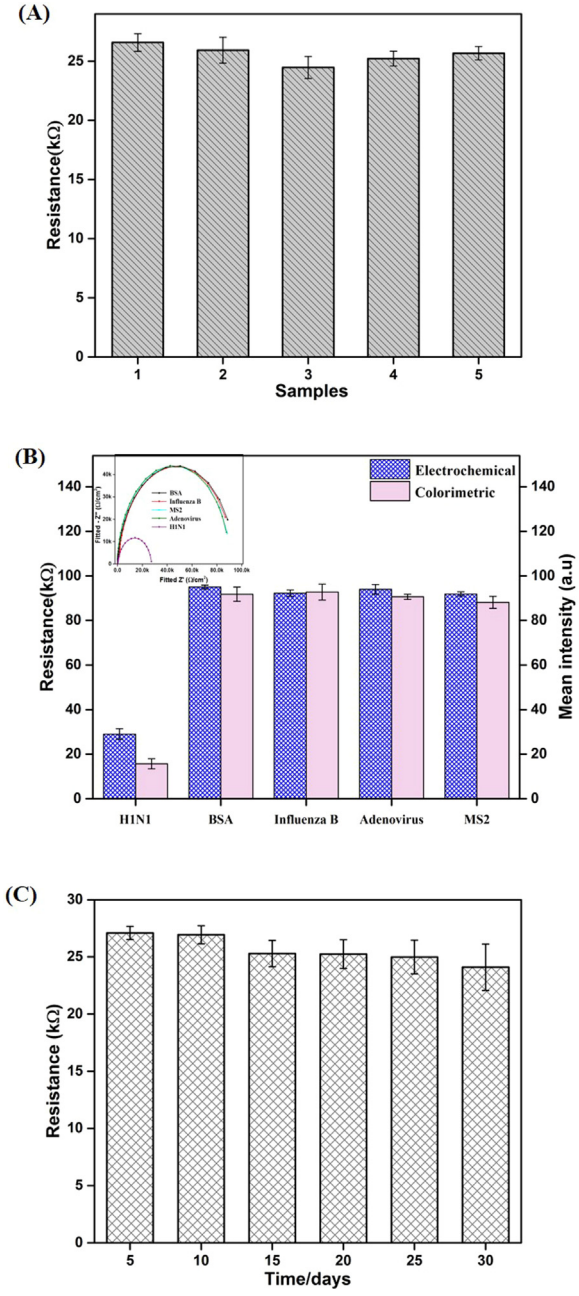

Fig. 5. (A) Repeatability of the immunosensors was evaluated using 2500 PFU mL^{-1} H1N1 virus concentration at five different electrodes. (B) Selectivity of the immunosensors was evaluated against bovine serum albumin (negative control), adenovirus, influenza B virus, and MS2 bacteriophages. The inset represents the respective Nyquist plot responses. (C) Stability of the immunosensors. The current responses of the electrodes were observed at intervals of five days for one month. The error bars represent the standard deviations of three independent measurements.

28.3 kΩ for the H1N1 virus, while they remained for the other viruses, showing the specificity of the immunosensors to H1N1 viruses.

The stability was also investigated at 2500 PFU mL^{-1} of the H1N1 virus (Fig. 5(C)). The resistance of the immunosensors maintained during the first five days, underwent a minor change of 5.7% at day 15, and retained 89.8% of its initial value for 30 days. The good stability can be attributed to the good SAM formation (Ahmad et al., 2016; Chira et al., 2012) and the gradual deactivation of the immobilized biomolecules. The reproducibility, selectivity, and stability indicate that the proposed immunosensor is suitable for the quantitative and qualitative detections of H1N1 viruses in real samples.

4. Conclusions

In this study, we presented a VFA-based immunosensor for the electrochemical and colorimetric detection of H1N1 viruses using a DP sample pad with large pores on the upper side and small pores on the lower side. This sample pad concentrated the antigen–antibody complexes on a conjugate pad, thereby providing fast detection (~6 min) and high sensitivity (the limit of detection was less than 5 PFU mL^{-1} for saliva samples) along with the simplicity of the paper sensor (no more than a typical sandwich ELISA-type paper immunosensor) for both detection methods. These are comparable to those of the previous highest-level electrochemical and colorimetric sensors for the detection of influenza A viruses using various substrates (Table S2). Moreover, this sample pad passed small-sized bio-particles such as viruses and filter out larger particles, which would be useful for the detection of viruses from real air samples because they consist of diversely sized particles. We will extend this study for the detection of multiple analytes with minimal manual processing.

Acknowledgements

This research was supported by the 2018 Research Fund (1.180015.01) of UNIST and by the Ministry of Science and ICT, Korea, under the ITRC (Information Technology Research Center) support program (IITP-2018-2017-0-01635) supervised by the IITP (Institute for Information and communications Technology Promotion). The authors would also like to acknowledge and thank the staff of the UNIST Central Research Facilities (UCRF) and Mr. Dinh Nhan Ngo for their helps in this study.

Appendix A. Supporting information

Supplementary data associated with this article can be found in the online version at doi:10.1016/j.bios.2018.10.008.

References

Adkins, J.A., Boehle, K., Friend, C., Chamberlain, B., Bisha, B., Henry, C.S., 2017. Anal. Chem. 89, 3613–3621. https://doi.org/10.1021/acs.analchem.6b05009.
Ahmad, A., Pui Kee, L., Sheryna Jusoh, N., 2016. Middle-East J. Sci. Res. 24, 2152–2158. https://doi.org/10.5829/idosi.mejsr.2016.24.06.23658.
Anderson, C.E., Holstein, C.A., Strauch, E.-M., Bennett, S., Chevalier, A., Nelson, J., Fu, E., Baker, D., Yager, P., 2017. Anal. Chem. 89, 6608–6615. https://doi.org/10.1021/acs.analchem.7b00769.
Chira, A., Covaci, O.-I., Radu, G.L., Radu, G.-L., 2012. UPB Sci. Bull. Ser. B 74.
Clarke, O.J.R., Goodall, B.L., Hui, H.P., Vats, N., Brosseau, C.L., 2017. Anal. Chem. 89, 1405–1410. https://doi.org/10.1021/acs.analchem.6b04710.
Cummins, B.M., Chinthapatla, R., Ligler, F.S., Walker, G.M., 2017. Anal. Chem. 89, 4377–4381. https://doi.org/10.1021/acs.analchem.6b04717.
de Oliveira, R.A.G., Camargo, F., Pesquero, N.C., Faria, R.C., 2017. Anal. Chim. Acta 957, 40–46. https://doi.org/10.1016/J.ACA.2017.01.002.
Du, D., Wang, J., Wang, L., Lu, D., Lin, Y., 2012. Anal. Chem. 84, 1380–1385. https://doi.org/10.1021/ac202391w.
Föllscher, W., 2013. Open Access Master's Theses.
Han, K.N., Choi, J.-S., Kwon, J., 2016. Report 6, 25710. https://doi.org/10.1038/srep25710.
He, Y., Wu, Y., Fu, J.-Z., Wu, W.-B., 2015. RSC Adv. 5, 78109–78127. https://doi.org/10.1039/C5RA09188H.
Hong, S., Bhardwaj, J., Han, C.-H., Jang, J., 2016. Environ. Sci. Technol. 22, 12365–12372. https://doi.org/10.1021/acs.est.6b03464.
Jauset-Rubio, M., Svobodová, M., Mairal, T., McNeil, C., Keegan, N., Saeed, A., Abbas, M.N., El-Shahawi, M.S., Bashammakh, A.S., Alyoubi, A.O., O´Sullivan, C.K., 2016. Sci. Rep. 6, 37732. https://doi.org/10.1038/srep37732.
Kim, H.U., Kim, H.Y., Kulkarni, A., Ahn, C., Jin, Y., Kim, Y., Lee, K.N., Lee, M.H., Kim, T., 2016. Sci. Rep. 6, 34587. https://doi.org/10.1038/srep34587.
Lee, S., Kim, G., Moon, J., 2013. Sensors 13, 5109–5116. https://doi.org/10.3390/s130405109.
Lim, W.Y., Goh, B.T., Khor, S.M., 2017. J. Chromatogr. B 1060, 424–442. https://doi.org/10.1016/j.jchromb.2017.06.040.
Liu, B., Du, D., Hua, X., Yu, X.-Y., Lin, Y., 2014. Electroanalysis 26, 1214–1223. https://doi.org/10.1002/elan.201400036.
Nikitin, N., Petrova, E., Trifonova, E., Karpova, O., 2014. Adv. Virol. 859090. https://doi.

org/10.1155/2014/859090.
Oh, Y.K., Joung, H.-A., Kim, S., Kim, M.-G., 2013. Lab Chip 13, 768. https://doi.org/10.1039/c2lc41016h.
Posthuma-Trumpie, G.A., Korf, J., van Amerongen, A., 2009. Anal. Bioanal. Chem. 393, 569–582. https://doi.org/10.1007/s00216-008-2287-2.
Robinson, J.L., Lee, B.E., Kothapalli, S., Craig, W.R., Fox, J.D., 2008. Clin. Infect. Dis. 47, e61–e64. https://doi.org/10.1086/529386.
Sajid, M., Kawde, A.-N., Daud, M., 2015. J. Saudi Chem. Soc. 19, 689–705. https://doi.org/10.1016/j.jscs.2014.09.001.
Sinawang, P.D., Rai, V., Ionescu, R.E., Marks, R.S., 2016. Biosens. Bioelectron. 77, 400–408. https://doi.org/10.1016/j.bios.2015.09.048.
Taubenberger, J.K., Morens, D.M., 2010. Public Health Rep. 16–26.
van der Meer, F.J.U.M., Orsel, K., Barkema, H.W., 2010. Can. Vet. J. 51, 56–62.
Yezli, S., Otter, J.A., 2011. Food Environ. Virol. https://doi.org/10.1007/s12560-011-9056-7.
Zhu, X., Shah, P., Stoff, S., Liu, H., Li, C., Zhu, C., Cheney, M.A., Wilson, L.J., Curley, S.A., 2014. Analyst 139, 2850. https://doi.org/10.1039/c4an00313f.